Simulations of two-dimensional turbulent convection in a density-stratified fluid

Tamara M. Rogers*
Astronomy and Astrophysics Department, University of California, Santa Cruz, California 95064

Gary A. Glatzmaier†
Earth Sciences Department, University of California, Santa Cruz, California 95064

S. E. Woosley‡
Astronomy and Astrophysics Department, University of California, Santa Cruz, California 95064
(Received 23 September 2002; published 26 February 2003)

High resolution computer simulations of two-dimensional convection using the anelastic approximation are presented. These calculations span Rayleigh numbers from 10^8–10^{12} for Prandtl number equal to unity, with the fluid density decreasing by a factor of 12 from the bottom to the top of the convection region. This range covers several decades in the ''hard'' turbulent regime. While many studies of this sort have been conducted for the Boussinesq approximation (i.e., no density stratification), we use the anelastic approximation with a significant density stratification in this turbulent regime. The convection is dominated by a large-scale coherent flow composed of ascending and descending superplumes. We find a power law exponent of 0.28 for the Nusselt-Rayleigh number scaling and a power law with exponent of 0.50 for the Reynolds-Rayleigh number scaling for the entire parameter space studied. These values are very similar to those determined experimentally and analytically for convection with no density stratification.

DOI: 10.1103/PhysRevE.67.026315 PACS number(s): 47.27.Eq

I. INTRODUCTION

Turbulent convection manifests itself in many science and engineering applications. Modeling it accurately is crucial in the understanding of the geodynamo, the solar dynamo, atmospheric and ocean circulations, and stellar convection, to name a few. Because of the nonlinearities and strong coupling inherent in the Navier-Stokes equations, the development of accurate numerical models has proven difficult, at best. Recently though, both numerical and experimental results have advanced our understanding of turbulence. Although simulations of real conditions in the interior of a star or planet are still out of reach, we can hope that certain relations apply throughout the turbulent regime. For example, it is expected that there is a power law relation between the Nusselt number (Nu), which is a measure of the global heat flux, and the Rayleigh number (Ra) , which is a measure of convective driving, that holds throughout the turbulent regime.

Determining the value of the exponent in this scaling relation has been the goal of many experimental and numerical studies. Most of these studies have been conducted for Rayleigh-Benard convection. Recent experiments [1,2] at high Ra have found robust Nu-Ra scalings that hold for many decades in the turbulent regime. The dependence on the Prandtl number (Pr), which measures the viscous to thermal diffusion, seems to vary with the Ra regime.

The classical analytic theory by Priestley [3] predicted a power law scaling $\mathrm{Nu} \propto \mathrm{Ra}^{1/3}$. This scaling is derived by assuming that the hot and cold plates of the Rayleigh-Benard cell do not communicate and, therefore, that the depth of the cell should not enter into the scaling relation. Early experiments seemed to confirm this exponent [4], but more recent experiments that were able to reach further into the turbulent regime yielded different results. In particular, recent experiments have noted the prominence of a dominant large-scale coherent flow. This large-scale flow could provide for the interaction of the top and bottom boundaries of the Rayleigh-Benard cell that was previously ignored. The persistence of this large-scale coherent flow could very well change the power law exponent in the Nu-Ra scaling relation. In fact, more recent experiments that observe this coherent flow also record exponents smaller than the classical $\frac{1}{3}$ relation, with most experiments giving a power law exponent of $\frac{2}{7}$ [1,2,5].

Some analytic theories have been put forth to explain this exponent [1,6,7]. The theory laid out in Shraiman and Siggia [6] assumes that the large-scale coherent flow sets up a thermal boundary that is nested within the viscous boundary layer. This theory suggests that the $\frac{2}{7}$ relation is controlled by the shear flow. A different derivation presented by Ref. [1] does not include the large-scale shear flow, but assumes that buoyancy accelerates detached plumes into the interior of the convective fluid. The region over which this acceleration occurs provides an intermediate length scale used to derive the $\frac{2}{7}$ relation. Exactly what drives this scaling relation is still an unanswered question. A comprehensive analytic study on Nu-Ra and Ra-Reynolds number (Re) scaling has been conducted by Grossman and Lohse [7]. In their theory a large-scale coherent roll is necessary, but different scalings are derived for different configurations of the boundary layers. They find different scaling laws hold in different Ra-Pr parameter space and their analytic scaling laws are consistent with experimental results at low and high Ra.

Because of the highly nonlinear nature of the Navier-Stokes equations and the broad range of length scales, it has

*Electronic address: tami@ucolick.org
†Electronic address: glatz@es.ucsc.edu
‡Electronic address: woosley@ucolick.org

been difficult to numerically study the same high Ra regimes as the experiments, but some attempts have been made. Kerr [8] conducted direct numerical simulations of Rayleigh-Benard convection in a (three-dimensional) 3D box for $5\times10^4\leqslant \mathrm{Ra}\leqslant 2\times10^7$. In that paper, a Nu-Ra scaling consistent with the experimental result of a power law exponent of $\frac{2}{7}$ was found. However, the large-scale coherent structure inherent in experimental results was not evident in the simulations. These simulations were limited to a low Ra regime, not quite reaching the ''hard'' turbulent regime.

Two-dimensional calculations, which of course are not as realistic, are able to reach higher Ra. The highest Ra simulations so far were conducted by Vincent & Yuen [9,10] and spanned $10^8\leqslant \mathrm{Ra}\leqslant 10^{14}$. These calculations found a Nu-Ra power law exponent of $\frac{1}{2}$ for Ra above 10^8, consistent with some analytic theories [11,7]. However, laboratory experiments at similar Ra do not reproduce this scaling law.

All of the aforementioned numerical studies were conducted using the Boussinesq approximation, which assumes no density stratification across the convective region. This approximation is well suited for the comparison of numerical work with experiments. However, atmospheres and interiors of stars and planets are compressible; and so for these problems it is more appropriate to use the anelastic approximation [12,13]. Here, we wish to gain some insight into how the turbulence is affected by compressibility. This could tell us how well laboratory experiments conducted with an essentially incompressible fluid are applicable to astrophysical and planetary problems.

II. NUMERICAL TECHNIQUE

Unlike the Boussinesq approximation, the anelastic approximation allows for a stratification in the background density and temperature. As in the Boussinesq case, this approximation is valid for fluids where convective speeds are much less than the speed of sound and the thermodynamic perturbations are small compared with the background state.

The Navier-Stokes equations using the anelastic approximation are

$$\vec{\nabla}\cdot\overline{\rho}\vec{v}=0, \tag{1}$$

$$\frac{\partial\vec{v}}{\partial t}+(\vec{v}\cdot\vec{\nabla})\vec{v}=-\vec{\nabla}P+\frac{S}{c_p}g\hat{z}+\overline{\nu}\left[\nabla^2\vec{v}+\frac{1}{3}\vec{\nabla}(\vec{\nabla}\cdot\vec{v})\right], \tag{2}$$

$$\frac{\partial S}{\partial t}+(\vec{v}\cdot\vec{\nabla})S=\frac{1}{\overline{\rho}\overline{T}}\vec{\nabla}\cdot\overline{\rho\kappa T}\vec{\nabla}S, \tag{3}$$

where $\vec{v}$ represents the fluid velocity, S represents the entropy perturbation, c_p is the (constant) specific heat at constant pressure, g is the constant gravitational acceleration, $\overline{\nu}$ is the kinematic viscosity, $\overline{\kappa}$ is the thermal diffusivity, P is the reduced pressure (pressure perturbation/$\overline{\rho}$ + gravitational potential perturbation) [14] and $\overline{\rho}$ and $\overline{T}$ represent the background density and temperature, respectively. Overbars refer to an adiabatic hydrostatic background state that is only a function of the vertical coordinate; all other variables are perturbations relative to this background state. We assume a Newtonian fluid with a constant dynamic viscosity ($\overline{\rho\nu}$). Since we are interested in stellar and planetary convection, our $\overline{\nu}$ and $\overline{\kappa}$ are assumed to be eddy diffusivities, which is why our diffusive heat flux in Eq. (3) is proportional to the gradient of entropy [14]. We also assume two-dimensional (x,z) solutions, i.e., no gradients or flow in the third dimension (y). The horizontal boundary conditions are periodic and the top and bottom boundary conditions are isentropic, stress-free, and impermeable.

For numerical simplification, we cast the momentum equation (2) in terms of a vorticity equation, where the vorticity is defined as

$$\vec{\omega}=\vec{\nabla}\times\vec{v}. \tag{4}$$

In addition, we define a stream function such that

$$\overline{\rho}\vec{v}=\vec{\nabla}\times\vec{\psi}. \tag{5}$$

By solving for mass flux via a stream function (5), conservation of mass (1) is ensured.

After taking the curl, the momentum equation becomes

$$\frac{\partial\omega}{\partial t}+(\vec{v}\cdot\vec{\nabla})\omega=h_\rho v_z\omega-\frac{g}{c_p}\frac{\partial S}{\partial x}+\overline{\nu}\vec{\nabla}^2\omega+\frac{\partial\overline{\nu}}{\partial z}\left(\vec{\nabla}^2 v_x-\frac{h_\rho}{3}\frac{\partial v_z}{\partial x}\right), \tag{6}$$

where h_ρ is the inverse of a density scale height $d\ln\overline{\rho}/dz$ and v_x and v_z are the x and z components of the velocity, respectively.

The vorticity and heat equations are solved using a Fourier spectral transform method in x and a finite difference method on a Chebyshev grid in z. The Chebyshev grid ensures the boundary layers are well resolved. Time advancing is done using the explicit second-order Adams-Bashforth method for the nonlinear terms and an implicit Crank-Nicolson method for the linear terms. The code is parallelized using MPI. The aspect ratio of the rectangular convecting region is set to two. For $\mathrm{Ra}=10^8$–10^{10} the resolution is 2048 grid points in x and 800 grid levels in z. For $Ra=10^{11}$–10^{12} the resolution is 4096 grid points in x and 2016 grid levels in z. For our highest Ra simulation, this resolution is barely adequate.

The kinematic viscosity and thermal diffusivity are inversely proportional to density ($\overline{\kappa},\overline{\nu}\propto\overline{\rho}^{-1}$) keeping the Pr constant in z and equal to unity. The Ra and Re are defined as

$$\mathrm{Ra}=\frac{g\Delta SD^3}{c_p\nu\kappa},\quad \mathrm{Re}=\frac{UD}{\nu}. \tag{7}$$

Here, D is the depth of the box, ΔS is the prescribed drop in entropy across D and U is the maximum vertical velocity, which is usually the velocity of the large-scale flow. All quoted Rayleigh numbers are the values at the bottom of the

box, where the Rayleigh number is the highest. Similarly the Reynolds number is calculated using the value of $\overline{\nu}$ at the bottom of the box. The Nu is defined as

$$\mathrm{Nu}=\frac{\left|\frac{\partial S}{\partial z}\right|_{bottom}}{\frac{\Delta S}{D}}. \tag{8}$$

We choose the background temperature, density, and pressure for our anelastic model to be described by a polytrope:

$$\overline{T}(z)=T_{bot}\left(1-\frac{z}{z_o}\right), \tag{9}$$

$$\overline{\rho}(z)=\rho_{bot}\left(1-\frac{z}{z_o}\right)^n, \tag{10}$$

$$\overline{p}(z)=p_{bot}\left(1-\frac{z}{z_o}\right)^{n+1}. \tag{11}$$

The polytropic index n, and the number of density scale heights across D, N_ρ, determine the constant z_o,

$$z_o=\frac{D}{1-e^{-N_\rho/n}}. \tag{12}$$

For the anelastic cases presented here, $n=\frac{3}{2}$ (ideal gas) and $N_\rho=2.5$ (i.e., the bottom density is ≈ 12 times greater than the top density).

III. RESULTS

We examined five anelastic cases (all with Pr=1): Ra $=10^8, 10^9, 10^{10}, 10^{11}$, and 10^{12}. The flow dynamics are dominated by one major ascending and expanding plume and one major descending and contracting plume, which dictate the large-scale coherent flow. Many other plumes rise from the boundary layer, but either detach or are swept by the large-scale wind into the main rising plume before they have a chance to rise very far.

The nature of these superplumes is similar to that described in Refs. [9,10]; it is characterized by a major plume with smaller plumes branching from it (Fig. 1). The superplumes are very structured and become even more structured on the small scale as the Rayleigh number is increased, as can be seen in Figs. 1 and 2. These superplumes are also concentrations of intense small-scale vorticity [15] and, as the Ra is increased, vorticity not only becomes more complex within the plume cores, but more coherent vortices are present throughout the simulated region as seen in Fig. 3.

All of these cases are technically in the ''hard'' turbulent regime [2], with Re varying from 10^4 to 10^6. Two-dimensional turbulence is marked by the simultaneous conservation of energy and enstrophy. The inertial range is dictated by downward enstrophy cascade with a k^{-3} energy dependence. Energy spectra for $10^9 \leqslant \mathrm{Ra} \leqslant 10^{12}$ are shown in Fig. 4. At $\mathrm{Ra}=10^9$ the kinetic energy spectrum follows the k^{-3} law quite well. As the Ra is increased the convective

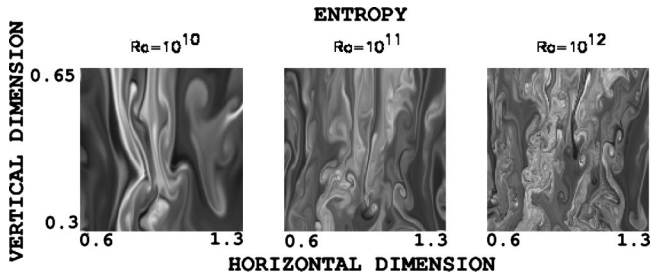

FIG. 1. Blow up of the descending plumes for the various Rayleigh numbers shown in Fig. 2. The size of these images is in terms of the total depth (D) of the convecting region.

driving causes the beginning of the inertial range to be shifted to larger wave number (smaller wavelengths). The majority of the resolution in these models is clearly used to discern the inertial range. In the highest Ra case, the wave numbers barely reach the dissipation range. To compare these models with traditional Rayleigh-Benard convection simulations and experiments, we calculated Nu-Ra and Re-Ra scalings. We find a Nu-Ra power law scaling of the form, $\mathrm{Nu}=0.53\mathrm{Ra}^{0.28}$ (Fig. 5), which matches the experimental $\frac{2}{7}$ scaling quite well [1].

For comparison, we have also run three Boussinesq models with Ra ranging from 10^9 to 10^{11} with Pr equal to unity.

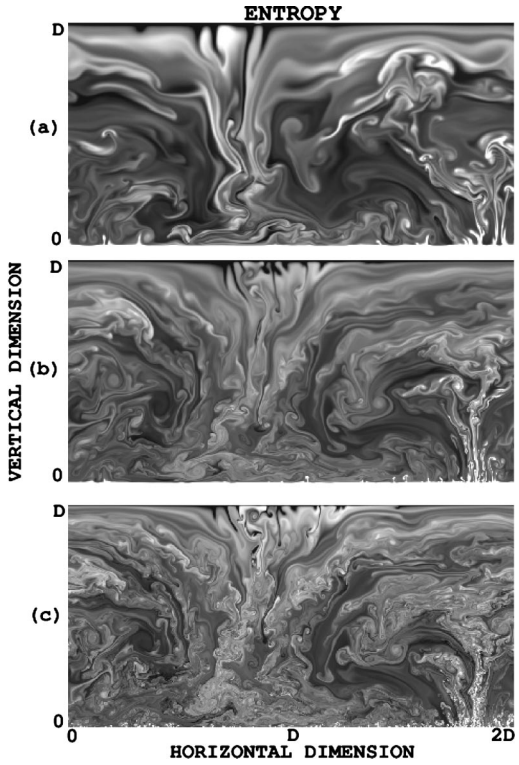

FIG. 2. Snapshots of the entropy perturbation with dark colors representing low entropy (i.e., cold heavy fluid) and light colors representing high entropy. (a) $\mathrm{Ra}=10^{10}$, superplume and branching plumes are seen, additional plumes rise (sink) from the bottom (top) of the cell but are swept into the major ascending (descending) plume by the large-scale flow (b) $\mathrm{Ra}=10^{11}$, (c) $\mathrm{Ra}=10^{12}$. This sequence illustrates how relative energy in the small scales increases with Rayleigh number.

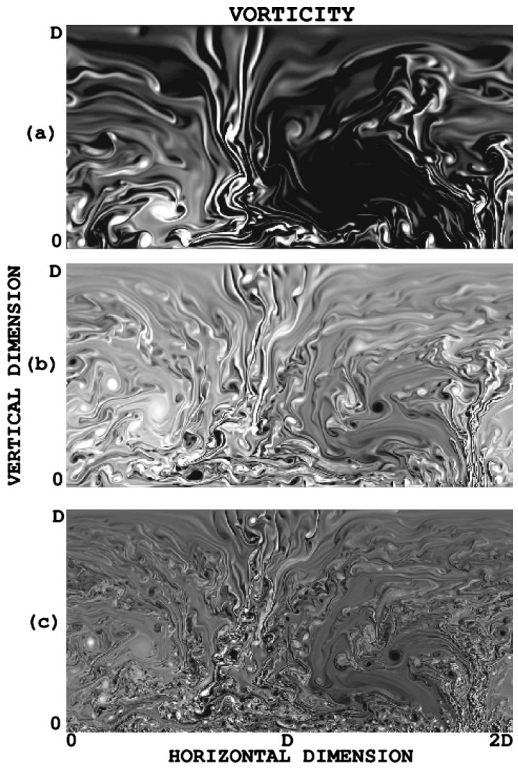

FIG. 3. Same as Fig. 2 except vorticity is plotted here. Clockwise flow is represented with light colors and counter-clockwise flow with dark colors. Strong coherent vortices are seen throughout. Concentrations of high vorticity occur in the rising and descending plumes.

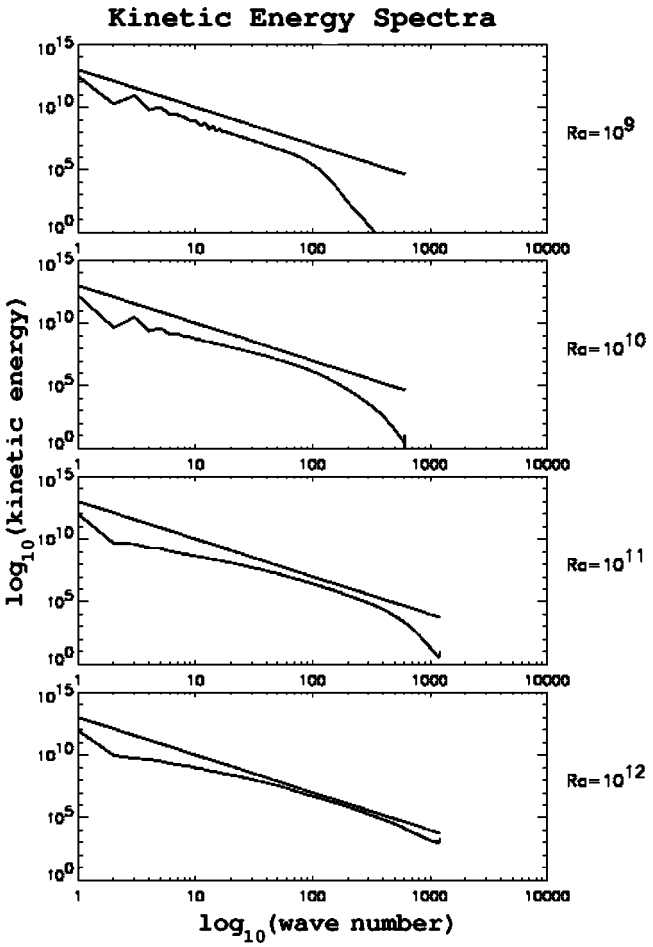

FIG. 4. Kinetic energy versus horizontal wave number for models with $10^9 \leqslant \mathrm{Ra} \leqslant 10^{12}$. Kinetic energy is normalized in each plot. These models are all clearly turbulent, with the inertial range matching the analytic k^{-3} slope (straight line).

In these models, we find a Nu-Ra scaling law $\mathrm{Nu} = 0.44\mathrm{Ra}^{0.29}$ as expected (Fig. 6). The comparison confirms that as far as the scaling laws are concerned, Boussinesq and anelastic approximations are similar. But, as can be seen in Fig. 7. the models are qualitatively quite different. The Boussinesq models are more top-bottom symmetric, due to the fact that the background density and viscous and thermal diffusivities are constant (unlike the anelastic approxiation). What is also very apparent is the fact that as the plumes rise in the Boussinesq fluid they do not expand and the mushroom cloud effect is missing. Because of this lack of expansion (contraction) the fluid looks more laminar than its anelastic counterpart.

The major differences between these models and those calculated by Refs. [9,10] are that these are anelastic and that these use a Chebyshev grid in the vertical direction which allows us to resolve the thermal boundary layer very well. In Fig. 8, it is obvious that the boundary layer is very thin, but because of the Chebyshev grid, we have 100 zones within this boundary layer. A uniform grid with the same total number of vertical zones would have only ten zones within the boundary layer. This fine resolution of the boundary layer may be crucial in distinguishing the $\frac{2}{7}$ relation from the $\frac{1}{2}$ relation.

One of the major questions regarding the Nu-Ra scaling is just what drives the $\frac{2}{7}$ scaling. The two main theories are that it is either (1) driven by the shear flow at the boundaries set up by the large-scale coherent flow or (2) dictated by the buoyant plumes. The boundary conditions in these models are stress-free; therefore, there is no traditional viscous boundary layer. The theory presented in [6] assumes that there is a thermal boundary layer nested inside the viscous boundary layer in order to arrive at the $\frac{2}{7}$ scaling relation. The results of our models seem to indicate that this is not necessary. Therefore, the large-scale coherent flow may not be the driving factor in the Nu-Ra relation. This is consistent with the experiment by Ciliberto *et al.* [16] in which the standard $\frac{2}{7}$ scaling law was reproduced even when the large-scale coherent flow was blocked. This indicates that either the buoyant plumes drive the scaling relation or that this scaling is robust and can be reproduced in many ways.

For $\mathrm{Ra} = 10^8 - 10^{10}$ and for $\mathrm{Pr} \approx 1$ Castaing *et al.* and Chavanne *et al.* [1,5] find a Re-Ra power law exponent of 0.49. Analytic models suggest an exponent of 0.50 [7]. We find this exponent to be 0.50 (Fig. 5) for our anelastic models and 0.49 (Fig. 6) for our Boussinesq models.

The proximity of these scaling relations to experimental and analytic work is unexpected, considering these models are for an anelastic gas with a significant density stratification in the vertical and that they are constrained to be two dimensional. In the analytic derivations by Grossman and

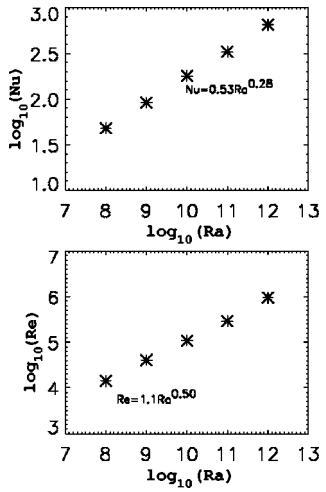

FIG. 5. $\log_{10}(\mathrm{Nu})$ versus $\log_{10}(\mathrm{Ra})$, similarly for Re-Ra. These plots show the Nu-Ra and Re-Ra scaling relations. No transition is detected up to $\mathrm{Ra}=10^{12}$ for either scaling relation.

Lohse [7], the fluid is assumed to be incompressible. Compressiblity would require an additional term in the energy dissipation; but this additional term behaves the same as the incompressible diffusion term and therefore does not affect the scaling law exponents. The equations for the thermal dissipation are the same as in the incompressible case with temperature replaced by entropy and the Nu redefined with respect to the entropy (8). Therefore, the scaling relations so derived for the anelastic case are the same as those for the Boussinesq. Clearly anelastic convection differs from Boussinesq (incompressible) convection in the details of the flow. Since in a fully compressible calculation, rising (sinking) plumes expand (contract) as in planetary atmospheres and stellar interiors. However, the total heat transfer, as measured by the Nu, is apparently little affected by this difference in flow structure.

It is important to recall that here we have assumed the fluid has constant dynamic viscosity and thermal conductivity. Other anelastic simulations with constant kinematic viscosity ($\overline{\nu}$) and thermal diffusivity ($\overline{\kappa}$) show somewhat different convective structures. In particular, there are more prominent small-scale plumes sinking from the top boundary (where the diffusivities are no longer large) [17].

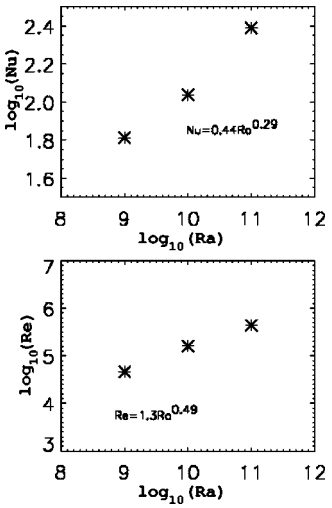

FIG. 6. Same as Fig. 5, except for Boussinesq models.

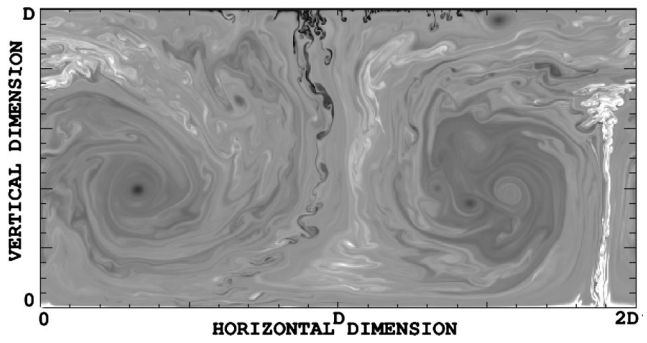

FIG. 7. Entropy perturbation for a Boussinesq simulation with $\mathrm{Ra}=10^{11}$. The entropy perturbation is directly proportional to the temperature pertubation in the Boussinesq approximation, with light colors representing warm fluid and dark colors representing cool fluid. Note the lack of expansion in the plumes that is seen in the anelastic case and the top-bottom symmetry that is lacking in the anelastic case.

One of the salient features of laboratory Rayleigh-Benard experiments has been the appearance of the large-scale coherent flow. This coherent flow could be a mechanism for inducing some two dimensionality in a three-dimensional flow. If this large-scale flow persists at even higher Rayleigh numbers it may be an indication that two-dimensional models of Rayleigh-Benard convection can provide accurate scaling laws for 3D laboratory experiments, as we have seen here.

IV. CONCLUSIONS

Our 2D anelastic convection for constant dynamic viscosity and thermal conductivity is dominated by a large-scale coherent flow similar to that observed in experiments. This coherent flow is shuttled by an ascending and descending superplumes, as seen in previous Boussinesq simulations.

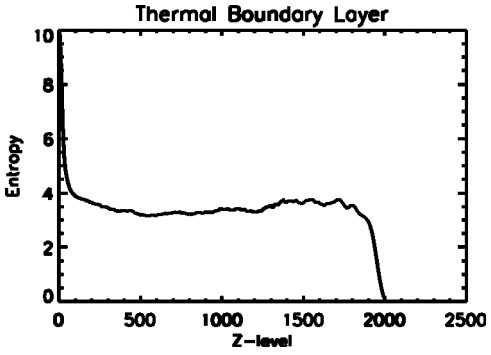

FIG. 8. The mean entropy for an anelastic model with $\mathrm{Ra}=10^{11}$ plotted versus the z-level number. The entropy here has been set to 0 at the top boundary and 10 at the bottom boundary. This prescribed ΔS helps determine the dimensionless Rayleigh number (7). Note, since a Chebyshev grid is employed in the model, the actual thermal boundary layer thickness is 1/200 of the depth and would not be perceptible in this plot if entropy were plotted versus the z coordinate.

The structure of these plumes, however, is qualitatively different because of the significant expansion of rising gas and contraction of sinking gas. Yet, quantitatively, we find that the Nu-Ra and Re-Ra scaling relations derived here are the same as those determined analytically for this Ra-Pr regime and that they are the same as those found experimentally. The fact that these models lack a viscous boundary layer, yet still yield the scaling relations found experimentally suggests that the driving mechanism of the $\frac{2}{7}$ scaling law does not require the nesting of the thermal boundary layer within the viscous boundary layer.

ACKNOWLEDGMENTS

This research was supported by the Scientific Discovery through Advanced Computing (SciDAC) Program of the DOE, DOE Grant No. DE–FC02-01ER41176, UC Research Partnership Initiatives Program, NSF Geophysics program, NASA Planetary Atmospheres program, and IGPP/LANL. The calculations were carried out on the NERSC supercomputer and on a Beowulf cluster provided by an NSF MRI grant. T.R. gratefully acknowledges the financial support from the National Physical Sciences Consortium.

[1] B. Castaing, G. Gunaratne, F. Heslot, L. Kadanoff, A. Libchaber, S. Thomae, X.Zh. Wu, S. Zaleski, and G. Zanetti, J. Fluid Mech. **204**, 1 (1989).
[2] F. Heslot, B. Castaing, and A. Libchaber, Phys. Rev. A **36**, 5870 (1987).
[3] C.H.B. Priestley, Austral. J. Physics **7**, 176 (1954).
[4] R.J. Goldstein, H.D. Chiang, and D.L. See, J. Fluid Mech. **213**, 111 (1990).
[5] X. Chavanne, F. Chilla, B. Chabaud, B. Castaing, and B. Hebral, Phys. Fluids **13**, 1300 (1997).
[6] B.I. Shraiman and E.D. Siggia, Phys. Rev. A **42**, 3650 (1990).
[7] S. Grossman and D. Lohse, J. Fluid Mech. **407**, 27 (2000).
[8] R.M. Kerr, J. Fluid Mech. **310**, 139 (1990).
[9] A.P. Vincent and D.A. Yuen, Phys. Rev. E **60**, 2957 (1999).
[10] A.P. Vincent and D.A. Yuen, Phys. Rev. E **61**, 5241 (2000).
[11] R.H. Kraichnan, Phys. Fluids **5**, 1374 (1962).
[12] Y. Ogura and N.A. Phillips, J. Atmos. Sci. **19**, 173 (1962).
[13] D.O. Gough, J. Atmos. Sci. **26**, 448 (1969).
[14] S.I. Braginsky and P.H. Roberts, GAFD **79**, 1 (1995).
[15] T. Cortese and S. Balachandar, Phys. Fluids A **5**, 3226 (1993).
[16] S. Ciliberto, S. Cioni, and C. Laroche, Phys. Rev. E **54**, 5901 (1996).
[17] M. Evonuk and G. A. Glatzmaier (private communication).